Available online at www.sciencedirect.com

jmr&t Journal of Materials Research and Technology

www.jmrt.com.br

Original Article

Experimental investigation of mechanical properties of cold-drawn AISI 1018 steel at high-temperature steady-state conditions

M. Badaruddin, H. Wardono, Zulhanif, H. Supriadi, M. Salimor*

Department of Mechanical Engineering, Faculty of Engineering, Universitas Lampung, Jalan Prof. S. Brojonegoro No. 1, Bandar Lampung 35145, Indonesia

ARTICLE INFO

Article history:
Received 5 March 2019
Accepted 6 December 2019
Available online 23 December 2019

Keywords:
AISI 1018 steel
Cold-drawing process
Mechanical properties
Dynamic strain ageing
Fire-safety design

ABSTRACT

Fire is one of the most serious problems that affect the integrity of building structures. It can cause significant degradation of the structural strength of steel over a short period prior to building collapse. This study conducted an extensive experimental program on the mechanical properties of AISI 1018 cold-drawn steel (CDS) at elevated temperatures using the steady-state method. The elastic modulus of CDS AISI 1018 underwent a reasonably rapid reduction at temperatures of 100–200 °C. At higher temperatures up to 500 °C, the steel exhibited slow reduction in its elastic modulus, whereas sharp reduction was observed at temperatures of 550–750 °C. In contrast, slow reduction in mechanical strength was observed at temperatures of 100–200 °C. At 300 °C, the mechanical strength increased gradually until it achieved a peak at 500 °C. This phenomenon was attributed to a dynamic strain ageing (DSA) effect that provided benefits in terms of increased mechanical strength and ductility, which were relatively higher than the mechanical strength at room temperature. Dimple fracture characteristics were observed in all samples tested at elevated temperatures. After raising the test temperature to 750 °C, subsequent reduction in the area of the lamellar pearlite phase boundary led to a spheroidization process followed by increased ductility. Prescriptive model predictions based on the experimental data series were proposed and important features regarding the DSA phenomenon were highlighted regarding fire-safety design when using CDS AISI 1018 in building construction.

1. Introduction

Current demand for steel is high because it is used in various forms in the construction of modern buildings, e.g., steel plates, round bars, steel wire rope, hot- and cold-rolled steel, and cold-drawn steel (CDS). The strength of the steel used in modern building structures should meet fire-safety design standards to ensure that in the event of a fire, structural collapse does not occur before all occupants have evacuated the building. Therefore, the performance of steel under fire conditions requires serious scientific research. Zong et al. [1] and Shakya and Kodur [2] both investigated the mechanical properties of cold-drawn wire strands with high carbon content of 0.810–0.840 wt% under high-temperature steady-state conditions. Under these conditions, the blue brittleness

* *Corresponding author.*
E-mail: mbruddin@eng.unila.ac.id (M. Badaruddin).

https://doi.org/10.1016/j.jmrt.2019.12.021

phenomenon in the steel wires occurred at temperatures of 200–300 °C, which caused the rapid degradation of mechanical strength followed by the loss of ductility and brittle fracture. Conversely, the blue brittleness effect that occurred in prestressed bars [3] with a carbon content of 0.280–0.330 wt% under quenching and tempering conditions resulted in a significant decrease in strength and ductility at temperatures of 300–500 °C. The differences in the temperature ranges regarding the occurrence of the blue brittleness phenomenon in the studied steel wires/bars is attributed to the martensite volume fraction in the initial microstructure, i.e., the volume fraction of martensite in the steel wires was greater than in the prestressed bars. Chen et al. [4] compared the performance of high-strength steel (HSS) BISPLATE 80 under quenching conditions with that of mild steel XLERPLATE grade 350 under normalizing conditions at temperatures of 22–1000 °C under steady- and transient-state conditions. The elemental alloys (e.g., manganese (Mn), molybdenum (Mo), and titanium (Ti)) in the XLERPLATE grade 350 were higher than in the BISPLATE 80. Their findings revealed similar slight reductions in both yield strength and elastic modulus for HSS and mild steel in the temperature range of 22–540 °C. Qiang et al. [5–7] evaluated the performance of HSS S460N under normalizing conditions and that of HSS S690Q and very high strength (VHS) S960Q steel under quenching and tempering conditions at steady-state temperatures in the range of 20–700 °C. The HSS S460N exhibited better performance at temperatures of 100–400 °C in comparison with the HSS S690Q and VHS S960Q. Diffusion of solute carbon atoms from martensite in the S690Q and VHS S960Q with relatively high chromium (Cr) and Mo contents at high temperatures resulted in poor performance with respect to fire resistance because of the formation of large precipitates in the shape of soluble carbides containing Cr and Mo [8]. This behaviour was similar to that of VHS-31.8 steel tubes manufactured via the quenching process [9]. In this case, the increase in large amounts of precipitate was caused by the outward diffusion of many solute carbon atoms from the solid solution of martensite, whereby the size and amount of precipitate were dependent on the elevated temperature. In addition, high (1.0 wt%) Mn content in HSS [6] and VHS steel grades [7–9] has also been found to contribute to the rapid degradation of mechanical strength via segregation of Mn from precipitates containing soluble Mn carbides leading to the formation of Mn–sulphide inclusions at various temperatures in the range of 100–400 °C [10].

Based on the above, it is evident that different manufacturing processes and different chemical compositions result in different microstructures of the tested steel products, which substantially determine the properties of the various steel grades. These two important factors have a considerable effect on the performance of steel grades at elevated temperatures. These factors are also the main reason that the current design standards of the American Institute for Steel Construction (AISC) and Eurocode cannot be applied to predict the reduction of mechanical properties for specific steel grades. For example, Qiang et al. [5] found the current design standard from the AISC [11] inappropriate for predicting the reduction factor of HSS S460N in terms of fire-safety design. Moreover, the model prediction of Eurocode 2 [12] could not capture certain important information, e.g., the strain hardening and blue brittleness effects experienced by cold-drawn wire strands at temperatures of 200–500 °C [2]. Consequently, different prediction models have been proposed and made available in the literature based on different steel grades, e.g., cold-drawn wire [1,2], cold-formed HSS SG550 grade (CFS SG550) [13,14], and VHS S960Q [7,9]. In addition, following a review of the experimental results of the data series in the literature, Maraveas et al. [15] proposed a simplified model for predicting the mechanical properties of HSS grades at elevated temperatures. However, few studies related to the mechanical properties of mild steel AISI 1018 manufactured via the cold-drawing process at elevated temperatures are available in the literature. High-strength CDS AISI 1018 in a round bar shape with highly deformed lamellar pearlite microstructures containing ferrite can be used in reinforced concrete structures, especially with a diameter of 5–12 mm as the main load-bearing bars of the slab members. In addition, cold-drawn steel tubes can be used as an alternative to welded and cold-rolled steel tubes because cold-drawn steel products exhibit narrower ranges of tolerance and section properties, which enables less machining and improved straightness. It is well known that at elevated temperatures, structural steel grades with ferrite–pearlite microstructures undergo lower reduction in steel strength than HSS and VHS steel grades with martensite microstructures [9]. Therefore, the study of the mechanical behaviour of CDS AISI 1018 at elevated temperatures regarding structural fire-engineering design applications is of considerable importance for providing data regarding cold-drawn AISI 1018 steel under steady-state high-temperature conditions.

In the present study, experiments were performed to investigate the mechanical properties of CDS AISI 1018 at temperatures in the range of 25–750 °C under steady-state conditions. The derived data were compared with existing data from the literature concerning high-temperature steady-state effects on cold-drawn wire strands [2], prestressed bars [3], HSS BISPLATE 80 [4], HSS S460N [5], HSS S690Q [6], CFS SG550 [13], and Q345 steel pipe [16]. The current model standards were established by AISC [11] for mild steel and by Eurocode 2 for cold-drawn steel wires [12]. The existing models proposed by other researchers [1,3,7,14,15] under steady-state temperature tests were also compared with the models proposed in the present work. Additionally, the steel microstructural changes and fractographic morphologies resulting from tensile tests were examined using an optical microscope and scanning electron microscopy (SEM) with secondary electron imaging, respectively, and discussed comprehensively.

2. Experimental procedure

2.1. *Materials and test equipment*

The present study used commercial cold-drawn AISI 1018 steel (CDS AISI 1018) round bars with 12-mm diameter. The chemical composition of the CDS AISI 1018 (wt%) was analysed using spark optical emission spectroscopy (Table 1). The specimens were obtained in accordance with ASTM E8M [17]. The dimensions and photographs of the specimens are presented in Fig. 1a and b, respectively. Analyses of the mechanical properties of the CDS AISI 1018 at both room temperature (RT) and

Table 1 – Chemical compositions of the CDS AISI 1018 (wt%).

C	Si	Mn	P	S	Al	Ti	Cu	Cr	Mo	Ni	Co	Nb	Fe
0.152	0.344	0.872	0.023	0.006	0.044	0.025	0.017	0.031	0.004	0.026	0.008	< 0.004	Bal.

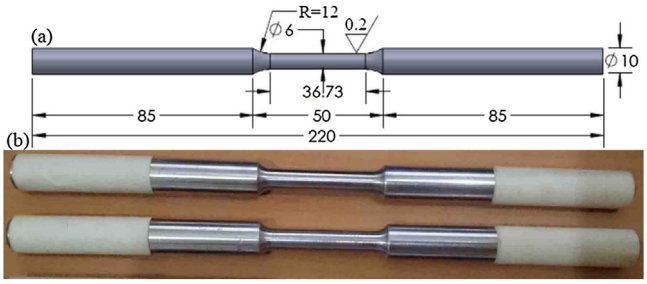

Fig. 1 – (a) Dimensions of the tensile specimens (all in mm) and (b) photographs of the specimens.

elevated temperatures were performed using a servohydraulic MTS Landmark with 100 kN capacity. An MTS 652.02 min. furnace with two hot zones and an MTS 653.02 controller with accuracy of ±1 °C were used for tensile testing at high temperatures. An MTS model 632.13F-20 with a 10-mm gauge length and an MTS model 632.54F-14 with a 12-mm gauge length were used for axial strain measurements at RT and high temperatures, respectively.

2.2. *Tension tests at elevated temperatures*

The tensile tests were performed at ambient (RT ≈ 25 °C) and elevated temperatures of 100–500 °C (in 100° increments) and 550–750 °C (in 50° increments). The strains were recorded incrementally using MTS model 634.13F-20 and MTS model 632.54F-14 extensometers at a sampling frequency of 10 Hz. Specimen temperatures were recorded using two thermocouples (XCIB K-type series from Omega) attached to the specimen in the gauge length region in accordance with ASTM E21 [18].

Each experiment was repeated three or seven times at the test temperatures, and the experimental details and number of specimens used in the experiments are listed in Table 2. For the tensile tests at high temperature, the test temperature for each specimen was achieved at a heating rate of 20 °C/min and then maintained for 35 min. Prior to commencing the tests, the extensometer was offset to zero and the specimen was pulled at a constant rate of 0.5 mm/min under displacement control until finished. Specimen temperature, strain, axial force, displacement, and run time were recorded using the data acquisition of the tensile template in MTS Multipurpose Elite software. The displacement movement at the constant rate of 0.5 mm/min resulted in a strain rate of approximately 0.7%/min in the specimen during tensile testing, which is the value recommended by ASTM E21 [18]. The axial extensometer was used only to 0.02 mm/mm for determining the elastic modulus and 0.2% yield strength. Further incremental strain after extensometer removal was calculated using the interpolation method and MTS Multipurpose Elite software based on the axial deformation of the specimens at a displacement rate of 0.5 mm/min. Sample microstructures in the fracture regions were examined using an Olympus optical microscope. The fractographs of the samples were characterized by means of SEM with secondary electron imaging signals (Carl Zeiss EVO MA 10, Germany).

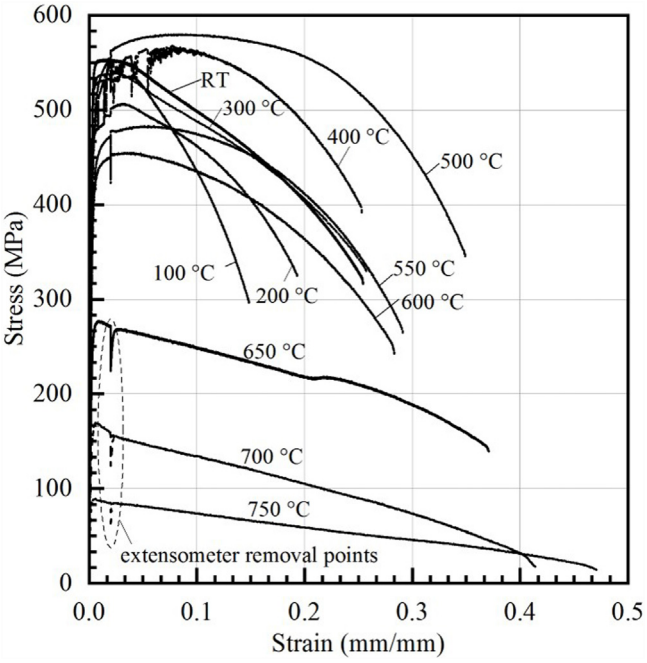

Fig. 2 – Typical stress–strain relationship curves for CDS AISI 1018 at elevated temperatures under steady-state conditions.

3. Results and discussion

3.1. *Temperature-related degradation of mechanical properties*

Typical engineering stress–strain curves for CDS AISI 1018 obtained from tensile tests conducted at temperatures of 25–750 °C are displayed in Fig. 2. The static drop evident in the figure due to extensometer removal from the specimen resulted in stress relaxation; however, this drop can be neglected [4]. The average values of the elastic modulus (E), yield strength (σ_y), and ultimate strength (σ_u) together with their standard deviation (STDEV) values over the temperature range of 25–750 °C are listed in Tables 3–5, respectively. Generally, after the cold-drawing process, the initial microstructure of the steel consisted of elongated grains of ferrite and pearlite in the longitudinal axis [19]. In addition, the lamellar cementite (Fe_3C) of the pearlite underwent severe deformation in the ferrite matrix, which led to carbon decomposition of the lamellar cementite and a decrease in the inter-phase spac-

Table 2 – The detailed number of specimens at different temperature tests.

Temperature (°C)	25	100	200	300	400	500	550	600	650	700	750
No. of specimens	7	3	6	4	5	5	4	6	3	4	3

Table 3 – The average values of elastic modulus with standard deviation (STDEV) values and its reduction factor of CDS AISI 1018.

T (°C)	25	100	200	300	400	500	550	600	650	700	750
E	197.07	186.71	176.83	177.26	174.44	171.25	168.54	158.32	133.72	97.92	80.67
STDEV	0.96	2.77	4.12	2.17	3.04	6.55	9.58	11.62	3.32	5.27	9.45
E_T/E	1.00	0.95	0.90	0.90	0.89	0.87	0.86	0.80	0.68	0.50	0.41

Table 4 – The average values of yield strength with STDEV values and its reduction factor of CDS AISI 1018.

T (°C)	25	100	200	300	400	500	550	600	650	700	750
σ_y	545.33	508.68	505.23	489.70	499.62	502.20	463.22	393.65	279.61	160.99	73.92
STDEV	7.01	28.16	22.85	23.23	15.57	20.23	37.80	73.43	30.74	9.24	21.79
$\sigma_{y,T}/\sigma_y$	1.00	0.93	0.93	0.90	0.92	0.92	0.85	0.72	0.51	0.30	0.14

Table 5 – The average values of ultimate strength with STDEV values and its reduction factor of CDS AISI 1018.

T (°C)	25	100	200	300	400	500	550	600	650	700	750
σ_u	550.64	524.34	525.94	529.66	554.12	580.06	531.30	445.64	296.81	171.88	84.99
STDEV	8.19	24.34	12.90	11.55	18.79	12.67	40.07	100.55	34.69	6.08	8.21
$\sigma_{u,T}/\sigma_u$	1.00	0.95	0.96	0.96	1.01	1.05	0.96	0.81	0.54	0.31	0.15

ing between the lamellar structures and ferrite [20]. Small inter-phase spacing provides a large boundary area, which constitutes an effective barrier to dislocation movement and leads to increased dislocation density. Thus, dislocation strain hardening generated large compressive residual stress in the axial direction [21] that increased the mechanical strength of the CDS AISI 1018 significantly. In contrast, steel has low capacity for plastic deformation during tensile deformation at RT, i.e., the stress–strain curve in the plastic region shows linear–plastic behaviour (Fig. 2). This characteristic is similar to that of both mild steel under cold-forming conditions [14] and steel wires under cold-drawing conditions [2]. In fact, during the cold-drawing process, the strength of steel wires was found to increase significantly through the collective contribution from the increased dislocation density, cementite deformation and decomposition, texture formation, and reduction of the inter-lamellar spacing in the pearlite.

Generally, the martensite phase in the initial microstructure of HSS [6,8] and VHS steel [7] grades under quenching and tempering conditions has been found largely responsible for the rapid degradation of the mechanical properties of such steel at low temperatures [9]. Martensite with highly effective interstitial carbon in the body-centred tetragonal structure is well known as the hardest, strongest, and most brittle phase; therefore, the phase has very low slip systems for dislocation motion during plastic deformation [22]. In addition, because of the low thermal stability of the martensite phase, outward diffusion of solute carbon atoms tends to occur easily to form precipitates of soluble carbides containing Cr or Mo [8]. These carbides are used by precipitates as a sink for alloy elements (e.g., Nb, Ni, and Ti) to form new larger precipitates that decrease the high-temperature resistance of the steel [23].

During the first stage of the experiments, the dependence of the mechanical strength and elastic modulus of CDS AISI 1018 on high-temperature steady-state conditions at temperatures in the range of 100–200 °C is shown in Fig. 3a and b, respectively. The high temperatures degraded the steel properties at a reasonably low rate, resulting in the decrease of the mechanical properties of CDS AISI 1018 steel with concurrent loss of ductility (Fig. 2). Characteristics similar to those of CDS AISI 1018 were found in HSS S460N by Qiang et al. [5], in which the rapid degradation could possibly be attributed to the blue brittleness effect. The blue brittleness effect is generally evident in hot-rolled steel under normalizing conditions at temperatures of 200–300 °C [24]. During the second stage, at temperatures of 300–400 °C (Fig. 3a), CDS AISI 1018 exhibited a gradual increase in mechanical strength; however, this increase was not followed by an increase in the elastic modulus (Fig. 3b). The occurrence of the serration phenomenon in the CDS AISI 1018, as shown in Fig. 2, indicates that the dynamic strain ageing (DSA) had begun in the steel. Onset of DSA is possible because of segregation of the solute of carbon atoms from Fe_3C precipitates, which leads to the diffusion into the partial dislocations in the ferrite matrix [25]. Furthermore, peak DSA in CDS AISI 1018, which occurred at 500 °C (Fig. 3a), led to increases in both mechanical strength and ductility, as shown in Fig. 2. This finding is similar to that reported by Lee et al. in relation to cold-drawn wire [26]. They found that temperatures in the range of 425–475 °C induced the diffusion of solute carbon atoms from the partially decomposed lamellar cementite in the highly deformed pearlite to ferrite dislocations. In contrast, Neuenschwander et al. [24] reported that DSA induced in hot-rolled S355 mild steel under normalizing conditions at 400 °C could be attributed to the high Mn content. However, the higher content (1.0 wt%) of Mn in HSS

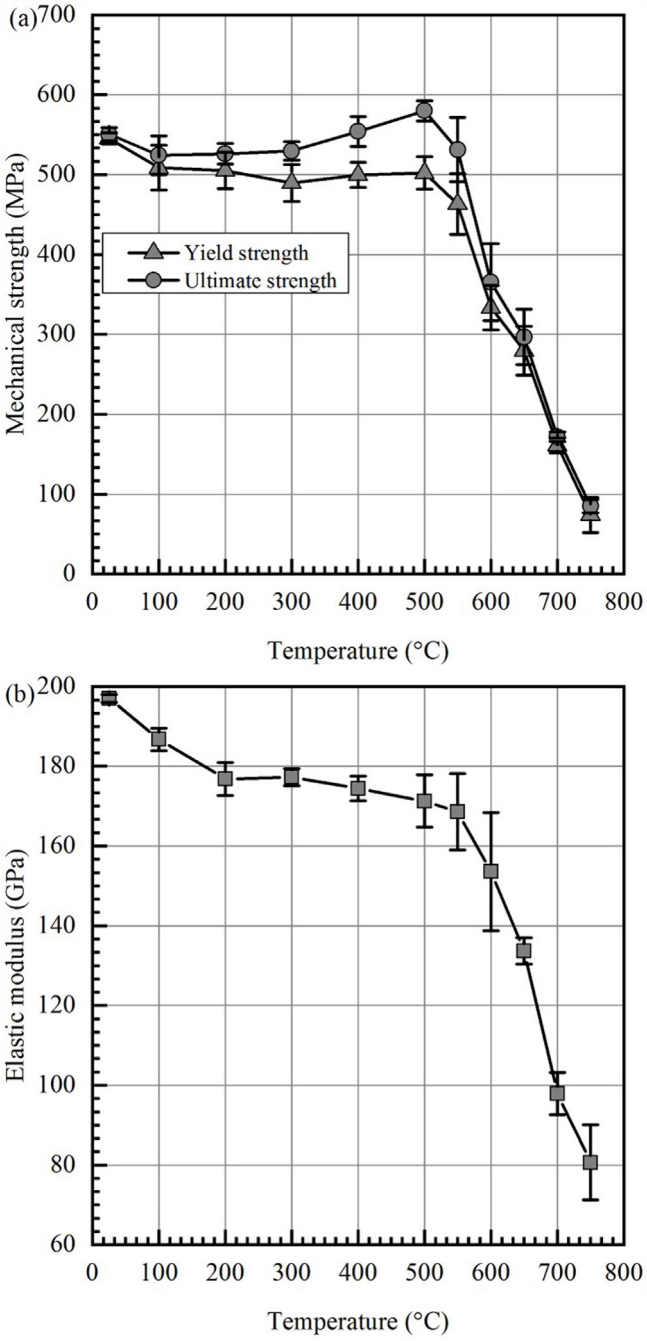

Fig. 3 – Dependence of (a) mechanical strength and (b) elastic modulus on temperature for CDS AISI 1018.

grades [5,6,8] leads to rapid degradation of the mechanical properties at an onset temperature of 400 °C. This explanation is supported by the findings of Maciejewski [10] who reported that higher (1.0 wt%) Mn content in high-strength mild steel grades leads to considerable anisotropy of tensile properties because of the formation of inclusions of elongated Mn sulphides during tensile deformation at 300 °C.

As mentioned above, strengthening in the mild AISI 1018 steel resulted in high dislocation density induced by strain hardening after the cold-drawing process. The increase in ultimate strength was due to the DSA effect at 500 °C. A temperature of 500 °C can cause increase in the lamellar inter-phase spacing, which leads to coarsening of lamellar structures in the ferrite region. Furthermore, effective dislocation locking occurred through coarsening of the lamellar structures and pinning by solute of the interstitial carbon from decomposition of the lamellar cementite in the ferrite matrix [26–28], which led to strain hardening in the steel. In addition, the elongated ferrite and pearlite grains facilitated many dislocations in the grain interior [29]. This explanation is evidenced by Fig. 2, in which plastic deformation can be observed through the non-linear plastic behaviour of the stress–strain relationship curve in the plastic region at 500 °C. Under the conditions of the third stage, rapid degradation of the mechanical properties of CDS AISI 1018 is evident in Fig. 3a and b. The tensile tests at temperatures in the range of 550–750 °C indicated that CDS AISI 1018 underwent continuous softening behaviour. It involved recovery and recrystallization that led to transformation from a lamellar to a spherical structure (spheroidization) [26], which led to decay of the mechanical properties of CDS AISI 1018 (Fig. 3a and b).

In the present study, reductions in the mechanical properties of CDS AISI 1018 at elevated temperatures under steady-state conditions were represented by reduction factor values. These were defined as the ratios of the mechanical properties at the elevated temperatures (E_T, $\sigma_{y,T}$, and $\sigma_{u,T}$) to those at RT (E, σ_y, and σ_u). The reduction factors corresponding to the temperatures are presented in Tables 3–5. Three predictive equations of reduction factors as functions of temperature (T) were obtained using the polynomial regression curve fitting method based on the experimental results. The accuracy of the equations, as determined by statistical analyses of the fitting of R^2, was approximately 98% and showed a reasonably good fit [2]. The present data and curve model predictions of the mechanical properties of CDS AISI 1018 at temperatures of 25–750 °C showed reasonable correlations (Fig. 4).

$$E_T/E = -6.481 \times 10^{-9}T^3 + 5.933 \times 10^{-6}T^2 - 1.688 \times 10^{-3}T + 1.048 \quad (25^\circ C \ll T \ll 750^\circ C) \tag{1}$$

$$\sigma_{y,T}/\sigma_y = -9.152 \times 10^{-9}T^3 + 7.639 \times 10^{-6}T^2 - 1.855 \times 10^{-3}T + 1.046 \quad (25^\circ C \ll T \ll 750^\circ C) \tag{2}$$

$$\sigma_{u,T}/\sigma_u = 6.860 \times 10^{-12}T^4 - 9.231 \times 10^{-9}T^3 + 5.245 \times 10^{-6}T^2 - 1.111 \times 10^{-3}T + 1.024 \quad (25^\circ C \ll T \ll 500^\circ C) \tag{3a}$$

$$\sigma_{u,T}/\sigma_u = 8.554 \times 10^{-8}T^3 - 1.649 \times 10^{-4}T^2 + 1.010 \times 10^{-1}T - 18.900 \quad (500^\circ\ C \ll T \ll 750^\circ\ C) \tag{3b}$$

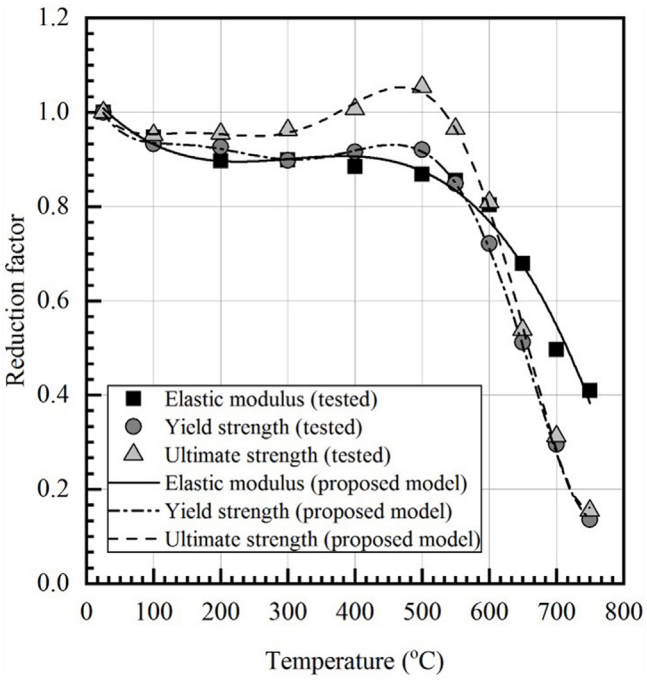

Fig. 4 – Comparisons of the elastic modulus, yield strength, and ultimate strength of the present data with the proposed models.

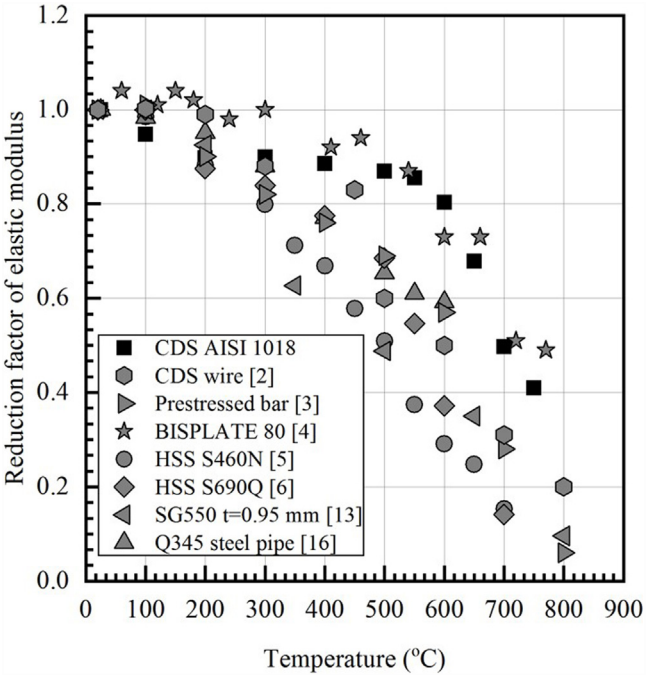

Fig. 5 – Comparison of reduction factor data of the elastic modulus of CDS AISI 1018 with literature data.

3.2. *Comparative analysis of test results with previous results*

3.2.1. *Elastic modulus*

As important material properties in terms of design parameters, the stiffness of steel and the capacities of load-bearing structures are influenced by the elastic modulus of steel at elevated temperatures. Therefore, quantitative or qualitative understanding of the reduction in the elastic modulus of steel under steady-state high-temperature conditions provides very important basic knowledge for evaluation of the fire-safety performance of structural steel. The reduction factor of the CDS AISI 1018 elastic modulus at various temperatures is shown in Fig. 4. As presented in Table 3, the elastic modulus of CDS AISI 1018 decreased with increasing temperature. For $T \leq 200\,^{\circ}C$, the elastic modulus decreased substantially, whereas it decreased relatively slowly at temperatures of 200–400 °C. Furthermore, at temperatures of 500–600 °C, the elastic modulus, E_T, gradually decreased. As the test temperature was increased to 750 °C, the CDS AISI 1018 steel underwent the most drastic deterioration in its elastic modulus via a decrease in the reduction factor of the elastic modulus of approximately 41% that at RT.

The test results of CDS AISI 1018 and the values from previous research studies on prestressed bars and CDS wire strands, Q345 steel pipe, and CFS SG550 and HSS grades are shown in Fig. 5. At 100 °C, the reduction in the elastic modulus for CDS AISI 1018 was higher value than that of the steels in previous studies [2–6,13,16]. For test temperatures of 400–750 °C, the results reported by Chen et al. [4] for HSS BISPLATE 80 agreed conservatively with the results of this experimental study. Moreover, at temperatures above 400–750 °C, the reductions in the values of the elastic modulus for prestressed bars [3], CDS wire strands [2], Q345 steel pipe [16], and CFS SG550 [13], HSS S460N [5], and S690Q [6] grades were remarkably higher than that of CDS AISI 1018. The differences between the reduction values of the elastic modulus for CDS AISI 1018 and the steels reported in previous research, as shown in Fig. 5, could possibly be attributable to the chemical composition of the micro-alloying elements and the carbon content in those steels that governed the temperature-related microstructural changes [30].

3.2.2. *Yield strength*

The yield strength of CDS AISI 1018 in the different temperature tests under steady-state conditions was consistently calculated based on a total strain of 0.2% [17]. As shown in Fig. 3a, the yield strength of CDS AISI 1018 showed reduction at a slow rate over temperatures in the range of 100–500 °C. For a test temperature of $500 < T < 600\,^{\circ}C$, the yield strength of CDS AISI 1018 showed gradual decrease in its reduction factor. In particular, for $T > 600\,^{\circ}C$, the yield strength decreased sharply. At $T = 650\,^{\circ}C$, the yield strength of 279.61 MPa was approximately 51% that at RT (545.33 MPa).

The reduction factor values for CDS AISI 1018 were compared with those of several typical prestressed bars, CDS wire strands, Q345 steel pipe, and CFS SG550 and HSS grades (Fig. 6). These comparisons show considerable discrepancy among the reduction factors of yield strength for prestressed bars [3] and CDS wire strands [2], Q345 steel pipe [16], and CFS SG550 [13] and HSS grades [4–6] based on tests at different temperatures. Furthermore, the reduction values for HSS S460N [5] were remarkably lower than for other steels [2–4,13,16]

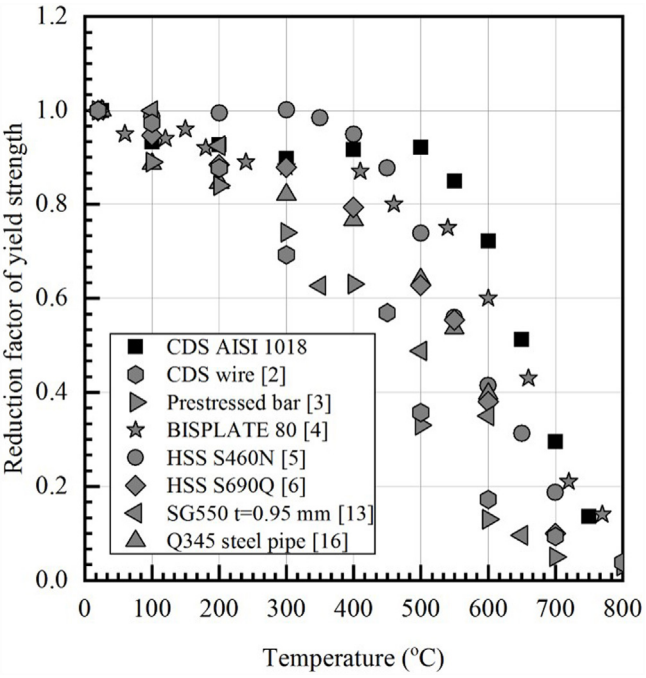

Fig. 6 – Comparison of reduction factor data of the yield strength of CDS AISI 1018 with literature data.

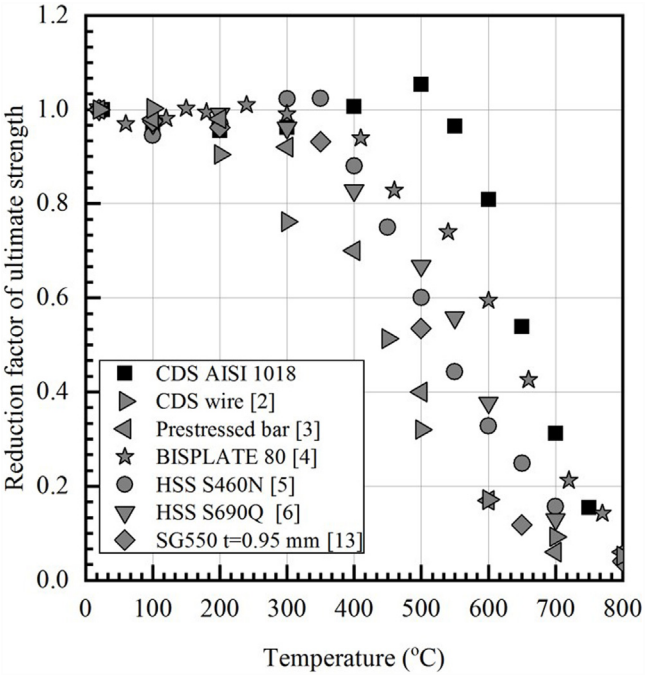

Fig. 7 – Comparison of reduction factor data of the ultimate strength of CDS AISI 1018 with literature data.

and the CDS AISI 1018 at temperatures of 200–400 °C (Fig. 6). The addition of micro-alloying elements such as Nb, V, Mo, Ti, and Ni to HSS S460N [5] yielded better steel performance than other steels at temperatures of 200–400 °C for which the presence of these elements in the steel delayed the recovery process by forming fine particle precipitations [31,32]. The decreases in the reduction values for the prestressed bars and CDS wire strands with increasing temperature were highly significant when compared with the values for CDS AISI 1018. The martensite phase formed in the initial microstructure of those steels has very low plastic deformation capacity with respect to tensile–plastic deformation under high temperature conditions, leading to continuous softening behaviour with increasing temperature [2,3]. Therefore, their mechanical properties decreased rapidly with increasing temperature, as shown in Fig. 6. In addition, CDS AISI 1018 exhibited slower reduction in yield strength than Q345 steel pipe [16] and CFS SG550 [13] and HSS [4–6] grades at temperatures of 500–700 °C.

3.2.3. *Ultimate strength*

The reduction factors of the ultimate strength of CDS AISI 1018 were compared with those of the prestressed bar, CDS wire strands, and cold-formed SG550 and HSS grades (Fig. 7). The reduction in the ultimate strength of CDS AISI 1018 occurred at a rate similar to CFS SG550 [13], HSS S460N [5], and HSS S690Q [6] at temperatures of 100–300 °C. However, the HSS S460N data [5] demonstrated a plateau or even a peak at temperatures of 200–300 °C, indicating that the blue brittleness phenomenon induced steel strength reduction. At the onset of the test at the temperature of 400 °C (Fig. 7), CDS AISI 1018 started to exhibit better performance than the other steel grades until the ultimate strength peaked at the magnitude of 1.0 at 500 °C because of DSA. Peak strain hardening in CDS AISI 1018 occurred at 500 °C and had beneficial effects regarding increases in both ultimate strength and ductility, which could be related closely to interactions of dissolved carbon atoms from highly deformed pearlite and dislocations in the ferrite matrix [26–28]. The reduction factor values corresponding to temperatures of 400 and 500 °C, shown in Fig. 7, indicate that DSA was induced in the CDS AISI 1018, similar to findings reported by Neuenschwander et al. [24]. The DSA effect could be included in the mathematical model for predicting the reduction factor of ultimate strength. Furthermore, the CDS wire strands and prestressed bars with martensite phase [2,3] exhibited sharp decrease in ultimate strength at the onset of 300 °C (Fig. 7), whereas the HSS grades [4–6,13] exhibited rapid reduction at the onset of 400 °C. The processes of manufacturing SG550 steel grade under cold-forming conditions [13], HSS S460N under normalizing conditions [5], HSS S690Q under quenching and tempering conditions [6], prestressed bars under quenching conditions [3], and steel wires under cold-drawing conditions [2] generate differences in the chemical composition of these steels, and results in considerable variation in their mechanical behaviour at elevated temperatures under steady-state conditions.

3.3. *Comparison of the proposed models with existing models and current model standards*

Comparisons of the proposed models, current model standards from the AISC [11] and Eurocode 2 [12], and existing models from the literature [1,3,7,14,15] for predicting the reduction in steel mechanical properties are presented in Fig. 8. Reductions in the elastic modulus and yield strength of cold-drawn AISI 1018 steel, prestressed bars, CDS wire strands, CFS G550, the HSS model, and VHS S960Q at different temper-

atures are shown in Fig. 8a and b, respectively. The reduction factors for the elastic modulus and yield strength were calculated using different models at temperatures in the range of 100–300 °C. The elastic modulus and yield strength calculated using the existing models from literature [1,3,7,14,15] yielded higher reduction factors at the highest temperature of 300 °C. Again, the reduction factor values for the elastic modulus and yield strength of CDS AISI 1018 calculated using the present models exhibited non-conservative properties in comparison with those calculated using design model standard from Eurocode 2 [12].

The reduction factors of ultimate strength at elevated temperatures calculated using different models varied considerably at temperatures of 100–400 °C (Fig. 8c). The reduction factor of ultimate strength calculated using the AISC [11] for mild steel was considerably lower predicted using the present model for CDS AISI 1018 at temperatures of 100–400 °C. Above this temperature, the existing models from the literature [1,3,7,14,15] and the current design standard of the AISC [11] resulted in higher predictions than the present model. In addition, the plot of a 0.6 reduction value to the present model prediction and to the model prediction of the AISC in Fig. 8c resulted in a critical temperature for CDS AISI 1018 (~644 °C) that was higher than predicted by the AISC for mild steel (~550 °C). The strength of any structural steel exposed to fire for a certain period must be retained to at least 60% that of its RT strength [11]. Based on this comparative analysis, significant differences attributable to steel properties and steel manufacturing processes imply that none of the aforementioned model predictions is applicable for fire-safety design of CDS AISI 1018. Therefore, the present data further emphasize the necessity for appropriate model predictions in the construction of building structures using CDS AISI 1018 rather than those based on prestressed bars and CDS wires, HSS grades, and VHS steel grades. The present model predictions could be used to predict reductions in the mechanical properties of CDS AISI 1018 at temperatures in the range of 100–750 °C.

3.4. *Dependence of microstructures and fractography on temperature*

The microstructure of CDS AISI 1018 is shown as a cross section of as-received steel in Fig. 9a. The light grains of ferrite and the lightly dark grains of pearlite colonies with relatively equiaxial morphology consisting of a lamellar cementite (Fe_3C) structure within a ferrite matrix can be observed. In addition, the fine dark phase evident at the grain boundaries is most likely due to carbides with elongated morphology along with grain boundary orientations, which precipitate as a second phase. This microstructure is similar to that of AISI 1016 produced under cold-drawing conditions, as examined using X-ray diffraction and SEM in Ref. [33]. After tensile deformation tests at both RT and elevated temperatures, optical microscope observations can distinguish the evolution of crystallized grains from the elongated deformed grains in the near-fracture region, as shown in Fig. 9b–d. The microstructure of the samples tested at RT (Fig. 9b) shows many more pearlite colonies than samples tested at 400 °C (Fig. 9c). The coarse grains observed in the microstructure illustrated in

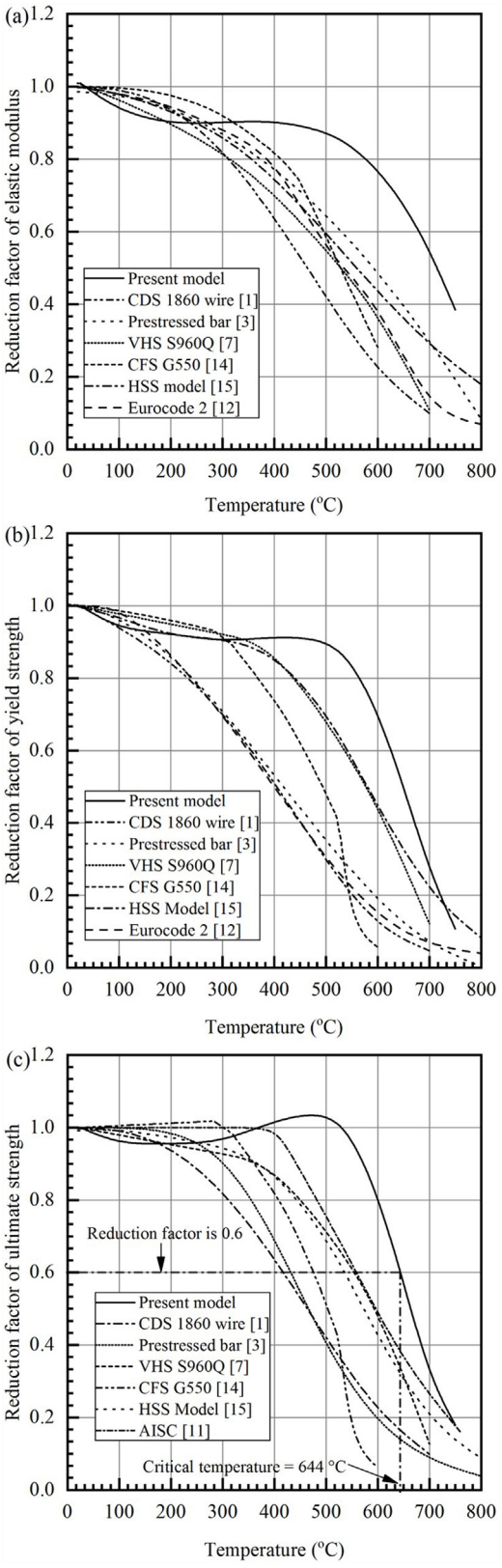

Fig. 8 – Comparison of the present models with existing models from the literature and the current model prediction for (a) elastic modulus, (b) yield strength, and (c) ultimate strength.

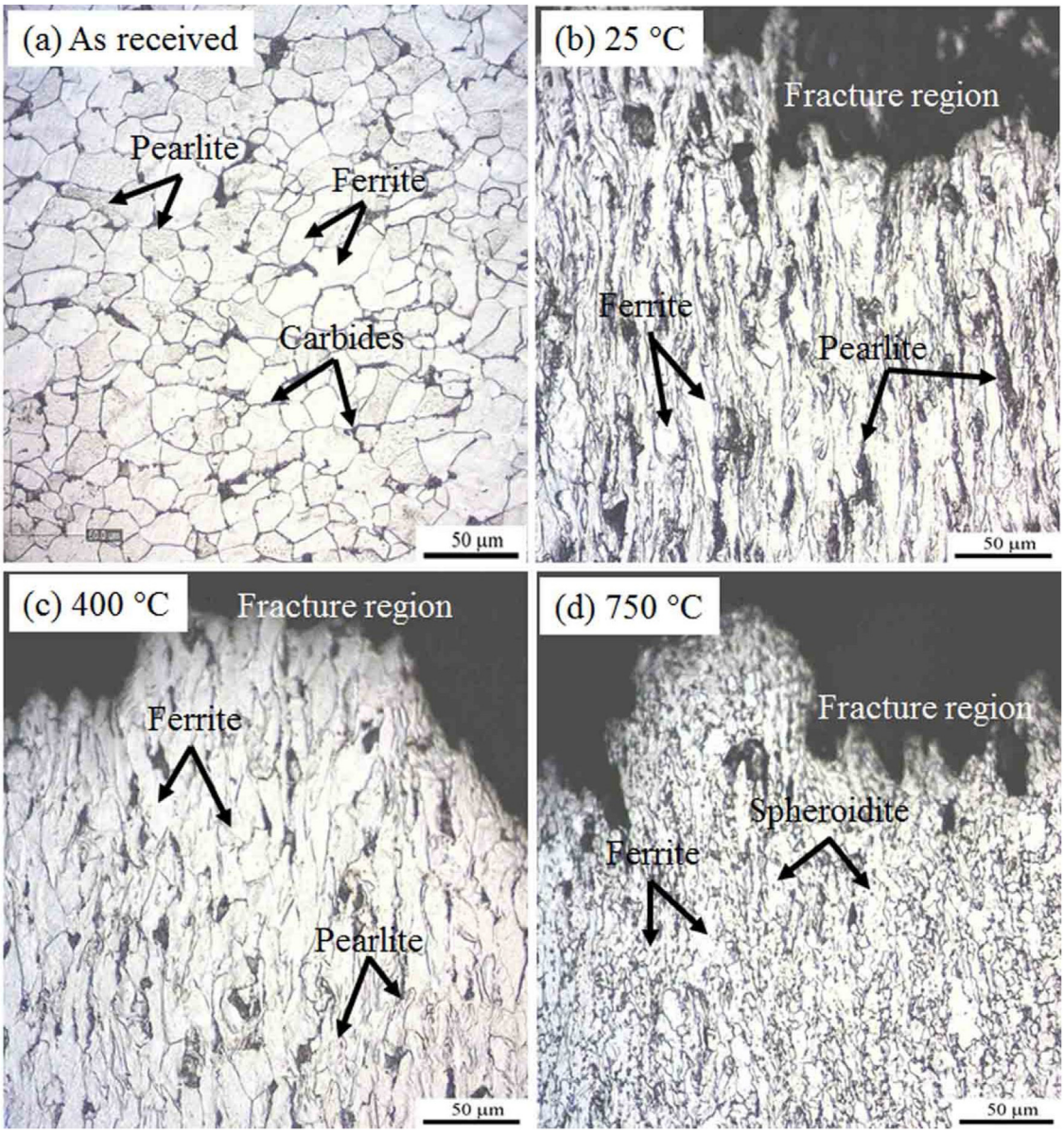

Fig. 9 – Microstructural evolution of CDS AISI 1018 in the fracture region after tensile tests at different temperatures.

Fig. 9c indicate that coarsening of the lamellar cementite structure led to reduction in the area of the phase boundary between the lamellar structure and the ferrite matrix. Furthermore, in the tensile temperature test at 750 °C, substantial changes in the microstructure evident in Fig. 9d imply that the cold-drawn AISI 1018 steel underwent significant softening behaviour, which could be related to the transformation of lamellar pearlite to sphere-like particles (spheroidite). This phenomenon is known as the spheroidization process, in which the driving force could be attributed to subsequent reduction in the area of the ferrite–lamellar cementite phase boundary [34]. This is considered the cause of the significant loss of mechanical strength in steel.

Fracture surface morphologies typical of CDS AISI 1018 specimens at low and high magnification after mechanical testing at different test temperatures are presented in Fig. 10. Despite ductility decrease or increase accompanied by loss of strain-hardening capacity, the fracture features present a ductile characteristic with numerous small and large dimples (Fig. 10a–d). Spherical crack areas at the surface fractures indicate that dimple fractures are controlled by nucleation, growth, and micro-void coalescence during the necking phenomenon of tensile deformation. Fracture morphology of the sample in Fig. 10a clearly shows numerous dimples with some smaller voids at the grain boundary and some larger voids in the pearlite regions. The voids nucleated and grew in regions of high stress concentration at the boundaries between the ferrite matrix and the grains [35] that consist of numerous carbide precipitates with high strain energy [36]. The fractograph of the sample tested at 200 °C shows fracture features similar to the sample tested at RT. However, only a few fine dimples observed under high magnification (Fig. 10b) can be attributed to the reduced capacity for plastic deformation, as indicated by the low ductility shown in Fig. 2.

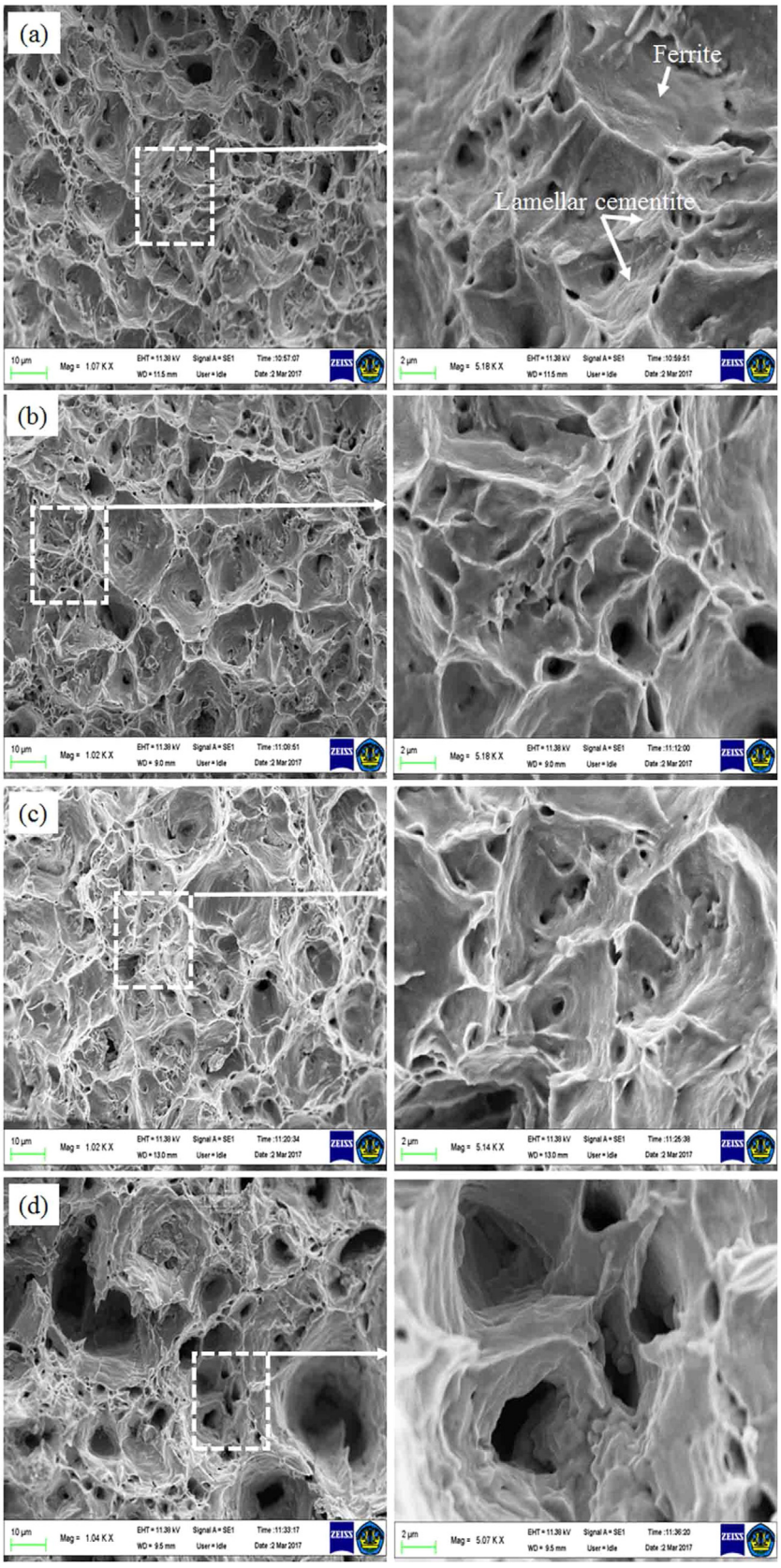

Fig. 10 – SEM surface fracture of CDS AISI 1018 after tensile tests at different temperatures: (a) RT, (b) 200 °C, (c) 500 °C, and (d) 750 °C. Dimples on the fracture surface are highlighted on the right-hand at higher magnification.

The significant differences in the surface fractures of samples tested at RT and samples tested at 500 and 750 °C could be related to the increase in dimple size with increasing temperature. The increased dimple size evident in the SEM fractographs of Fig. 10c and d reflect the coarsening of the microstructures that occurred during tensile deformation, indicating that recovery and recrystallization had begun. This is similar to observations of the fracture surface of VHS-31.8 steel tubes at temperatures of 100–600 °C [9]. Relatively coarser dimples with larger-sized voids, evident in Fig. 10c, resulted from numerous voids that merged and grew in the ferrite region consisting of lamellar cementite and rearrangement dislocations, which was then followed by a significant increase in ductility [37]. At 550 °C, recovery and recrystallization processes had begun, as indicated by the rapid reduction of the mechanical properties of CDS AISI 1018 shown in Fig. 3, which continuously facilitated the number of solutes of carbon atoms diffused into the lamellar cementite with low strain energy [26]. During the diffusion of solute carbon atoms, vacancies grew progressively and coalesced, resulting in voids with larger diameter and greater depth that acted as crack initiation points in the ferrite region. Regardless of the increase in test temperature, the shapes and sizes of the dimples varied with temperature up to 750 °C, as evidenced under high magnification (Fig. 10d).

4. Conclusions

This study investigated the mechanical behaviour of CDS AISI 1018 based on tensile tests over a temperature range of 100–750 °C under steady-state conditions. Reduction factor data for the elastic modulus and both yield and ultimate strengths were obtained and used to propose a new empirical equation for material model predictions. The mechanical properties of CDS AISI 1018 exhibited relatively higher reductions at temperatures of 100–200 °C than HSS grades and VHS steel grades. Beyond this temperature range, CDS AISI 1018 exhibited a relatively better performance in mechanical strength and elastic modulus. The effects of temperature on the reduction in mechanical strength and ductility was possible due to the blue brittleness phenomenon during the 200–300 °C test; however, the mechanical strength and ductility increased gradually at temperatures of 400–500 °C. This finding was attributable primarily to the delay of the recovery process by the diffusion of the solute of carbon atoms from decomposition of lamellar pearlite through the DSA mechanism. At temperatures above 550 °C, coarsening of the lamellar phase boundary area in the ferrite matrix led to microstructural changes, which significantly affected the rapid reduction in mechanical steel properties. The critical temperature of CDS AISI 1018 obtained by fixing the reduction factor value to 0.6 was approximately 644 °C. This was higher than the critical temperature obtained from existing model predictions for prestressed bars, CDS wire strands, HSS grades, and VHS steel grades and from predictions of the AISC model for mild steel. The proposed models for prediction of the high-temperature mechanical properties of CDS AISI 1018 could be used to evaluate the response of CDS AISI 1018 structures in a fire if the thermal creep effect is not significant.

Conflict of interest

The authors declare no conflicts of interest in this article

Acknowledgments

This work was financially supported by the Ministry of Research, Technology, and Higher Education of Republic of Indonesia, the General Directorate of Research Strengthening and Development, the Directorate of Research and Community Service (DRPM) via the basic research grant under contract no. 065/SP2H/LT/DRPM/2019.

REFERENCES

[1] Zong Z, Jiang D, Zhang J. Study of the mechanical performance of Grade 1860 steel wires at elevated temperatures. Mater Res Innov 2015;19(5):1175–6.
[2] Shakya AM, Kodur VKR. Effect of temperature on the mechanical properties of low relaxation seven-wire prestressing strand. Constr Build Mater 2016;124, 74–10.
[3] Hou X, Zheng W, Kodur V, Sun H. Effect of temperature on mechanical properties of prestressing bars. Constr Build Mater 2014;61:24–8.
[4] Chen J, Young B, Uy B. Behavior of high strength structural steel at elevated temperatures. J Struct Eng 2006;132(12), 1948–6.
[5] Qiang X, Bijlaard FSK, Kolstein H. Deterioration of mechanical properties of high strength structural steel S460N under steady state high temperature condition. Mater Des 2012;36, 438–4.
[6] Qiang X, Bijlaard F, Kolstein H. Dependence of mechanical properties of high strength steel S690 on elevated temperatures. Constr Build Mater 2012;30:73–6.
[7] Qiang X, Jiang X, Bijlaard FSK, Kolstein H. Mechanical properties and design recommendations of very high strength steel S960 in fire. Eng Struct 2016;112, 60–10.
[8] Neuenschwander M, Scandella C, Knobloch M, Fontana M. Modeling elevated-temperature mechanical behavior of high and ultra-high strength steels in structural fire design. Mater Des 2017;136, 81–21.
[9] Heidarpour A, Tofts NS, Korayem AH, Zhao XL, Hutchinson CR. Mechanical properties of very high strength steel at elevated temperatures. Fire Saf J 2014;64:27–8.
[10] Maciejewski J. The effects of sulfide inclusions on mechanical properties and failures of steel components. J Fail Anal Prev 2015;15, 169–9.
[11] AISC 360. Specification for structural steel building. United States of America: American Institute of Steel Construction Inc.; 2005.
[12] CEN. Eurocode 2: design of concrete structures: part 1-2: general rules-Structural fire design. British Standards Institution; 2004.
[13] Ranawaka T, Mahendran M. Experimental study of the mechanical properties of light gauge cold-formed steels at elevated temperatures. Fire Saf J 2009;44, 219–10.
[14] Wei C, Jihong Y. Mechanical properties of G550 cold-formed steel under transient and steady state conditions. J Constr Steel Res 2012;73:1–10.
[15] Maraveas C, Fasoulakis ZC, Tsavdaridis KD. Mechanical properties of high and very high steel at elevated temperatures and after cooling down. Fire Sci Rev 2017;6:1–12.

[16] Yuan G, Shu Q, Huang Z, Li Q. An experimental investigation of properties of Q345 steel pipe at elevated temperatures. J Constr Steel Res 2016;118:41–7.
[17] ASTM E8 M, ASTM International, West Conshohocken, PA, United States Standard test methods for tension testing of metallic materials; 2004.
[18] ASTM E21, ASTM International, West Conshohocken, PA, United States Standard Test methods for elevated temperature tension tests of metallic materials; 2005.
[19] Tao Z. Mechanical properties of prestressing steel after fire exposure. Mater Struct 2015;48, 3037–10.
[20] Zhang X, Hansen N, Godfrey A, Huang X. Dislocation-based plasticity and strengthening mechanisms in sub-20 nm lamellar structures in pearlitic steel wire. Acta Mater 2016;114:176–7.
[21] Sato S, Wagatsuma K, Suzuki S, Kumagai M, Imafuku M, Tashiro H, et al. Relationship between dislocations and residual stresses in cold-drawn pearlitic steel analyzed by energy-dispersive X-ray diffraction. Mater Charact 2013;83:152–8.
[22] Badaruddin M, Sugiyanto H Wardono, Andoko CJ Wang, Rivai AK. Improvement of low-cycle fatigue resistance in AISI 4140 steel by annealing treatment. Int J Fatigue 2019;125:406–11.
[23] Karthikeyan S, Viswanathan GB, Gouma PI, Vasudevan VK, Kim YW, Mills MJ. Mechanisms and effect of microstructure on creep of TiAl-based alloys. Mater Sci Eng A 2002;329–331:621–9.
[24] Neuenschwander M, Knobloch M, Fontana M. Elevated temperature mechanical properties of solid section structural steel. Constr Build Mater 2017;149, 186–15.
[25] Hong S, Shin SY, Lee J, Ahn DH, Kim HS, Kim SK, et al. Serration phenomena occurring during tensile tests of three high-manganese twinning-induced plasticity (TWIP) steels. Metall Mater Trans A 2014;45, 633–13.
[26] Lee JW, Lee JC, Lee YS, Park KT, Nam WJ. Effects of post-deformation annealing conditions on the behavior of lamellar cementite and the occurrence of delamination in cold drawn steel wires. J Mater Process Technol 2009;209:5300–4.
[27] Joung SW, Kang UG, Hong SP, Kim YW, Nam WJ. Aging behavior and delamination in cold drawn and post-deformation annealed hyper-eutectoid steel wires. Mater Sci Eng A 2013;586:171–6.
[28] Hosseini S, Heidarpour A, Collins F, Hutchinson CR. Strain ageing effect on the temperature dependent mechanical properties of partially damaged structural mild-steel induced by high strain rate loading. Constr Build Mater 2016;123:454–9.
[29] Jaya BN, Goto S, Richter G, Kirchlechner C, Dehm G. Fracture behavior of nanostructured heavily cold drawn pearlitic steel wires before and after annealing. Mater Sci Eng A 2017;707:164–7.
[30] Sawada K, Ohba T, Kushima H, Kimura K. Effect of microstructure on elastic property at high temperatures in ferritic heat resistant steels. Mater Sci Eng A 2005;394, 36–6.
[31] Ghosh S, Mula S. Thermomechanical processing of low carbon Nb–Ti stabilized microalloyed steel: microstructure and mechanical properties. Mater Sci Eng A 2015;646, 218–15.
[32] Lino R, Guadanini LGL, Silva LB, Neto JGC, Barbosa R. Effect of Nb and Ti addition on activation energy for austenite hot deformation. J Mater Res Technol 2019;8:180–8.
[33] Marulanda DM, Cuellar J, Rojas C, Acosta LM. Microstructure and mechanical properties of cold drawn AISI 1016 steel processed by ECAP. Univ Sci 2014;19(2), 139–7.
[34] Zhang MX, Kelly PM. Crystallography of spheroidite and tempered martensite. Acta Mater 1998;46(11), 4081–10.
[35] Komori K. Predicting ductile fracture in ferrous materials during tensile tests using an ellipsoidal void model. Mech Mater 2017;113, 24–19.
[36] Kumar MV, Balasubramanian V, Rao AG. Hot tensile properties and strain hardening behaviour of Super 304HCu stainless steel. J Mater Res Technol 2017;6(2), 116–6.
[37] Mirmomeni M, Heidarpour A, Zhao XL, Hutchinson CR, Packer JA, Wu C. Fracture behaviour and microstructural evolution of structural mild-steel under the multi-hazard loading of high-strain-rate load followed by elevated temperature. Constr Build Mater 2016;122, 760–11.